Simultaneously defining cell phenotypes, cell cycle, and chromatin modifications at single-cell resolution

Allison B. Chambliss,[*,†,‡] Pei-Hsun Wu,[*,†,‡] Wei-Chiang Chen,[*,†,‡] Sean X. Sun,[†,‡,§] and Denis Wirtz[*,†,‡,1]

[*]Department of Chemical and Biomolecular Engineering, [†]Physical Sciences-Oncology Center, [‡]Institute for NanoBioTechnology, and [§]Department of Mechanical Engineering, The Johns Hopkins University, Baltimore, Maryland, USA

ABSTRACT **Heterogeneity of cellular phenotypes in asynchronous cell populations placed in the same biochemical and biophysical environment may depend on cell cycle and chromatin modifications; however, no current method can measure these properties at single-cell resolution simultaneously and *in situ*. Here, we develop, test, and validate a new microscopy assay that rapidly quantifies global acetylation on histone H3 and measures a wide range of cell and nuclear properties, including cell and nuclear morphology descriptors, cell-cycle phase, and F-actin content of thousands of cells simultaneously, without cell detachment from their substrate, at single-cell resolution. These measurements show that isogenic, isotypic cells of identical DNA content and the same cell-cycle phase can still display large variations in H3 acetylation and that these variations predict specific phenotypic variations, in particular, nuclear size and actin cytoskeleton content, but not cell shape. The dependence of cell and nuclear properties on cell-cycle phase is assessed without artifact-prone cell synchronization. To further demonstrate its versatility, this assay is used to quantify the complex interplay among cell cycle, epigenetic modifications, and phenotypic variations following pharmacological treatments affecting DNA integrity, cell cycle, and inhibiting chromatin-modifying enzymes.—Chambliss, A. B., Wu, P.-H., Chen, W.-C., Sun, S. X., Wirtz, D. Simultaneously defining cell phenotypes, cell cycle, and chromatin modifications at single-cell resolution. *FASEB J.* 27, 2667–2676 (2013). www.fasebj.org**

Key Words: epigenetics · high-throughput · microscopy

Chromatin-associated modifications, such as histone acetylation and DNA methylation, regulate gene expression without altering underlying nucleotide sequences. Some of these modifications may be epigenetically inherited. In the nucleus, DNA is packaged into chromatin by wrapping around nucleosomes consisting of two copies each of histones H2A/B, H3, and H4. The reversible modification of these histones by acetyl groups plays a key role in modulating chromatin conformation (1). Low levels of histone acetylation correspond to compact chromatin conformation (heterochromatin) and low transcriptional activity, while high levels of histone acetylation correspond to open chromatin conformation (euchromatin) and high transcriptional activity. Acetylation levels are determined by the balancing activity of histone acetyltransferase enzymes (HATs) and histone deacetylase enzymes (HDACs) (2, 3).

Numerous studies have suggested a link between altered histone modification activity and disease state, in particular cancer (4–6). For instance, global levels of acetylation and dimethlylation on histones H3 and H4 are predictive of clinical outcome in primary prostate cancer tissues (7). Increased expression levels of several HDAC proteins, leading to histone hypoacetylation, are associated with disease advancement and poor prognosis in colorectal and gastric cancers (8), while histone H4 deacetylation at lysine 16 is common in a wide variety of cancer cells (9). A reversal of hypoacetylation, by way of HDAC inhibition, could be an effective treatment option for cancer patients (10, 11).

Current techniques to study chromatin-associated modifications, and specifically histone acetylation, include Western blot analysis (12), flow cytometry (13), immunohistochemistry (7), and genomic methods such as chromatin immunoprecipitation (9, 14, 15). Western blot approaches yield only relative, bulk-averaged acetylation values, and while genomic approaches provide locus-specific modification status at high resolution, they also rely on information averaged over a population of cells. Both of these approaches fail to recognize the potential heterogeneity of acetylation within a cell population. Flow cytometry attempts to capture cellular heterogeneity, but, like Western blot analysis and

Abbreviations: AcH3, acetylated histone H3; AcH4, acetylated histone H4; CV, coefficient of variation; DMSO, dimethyl sulfoxide; F-actin, filamentous actin; HAT, histone acetyltransferase enzyme; HDAC, histone deacetylase enzyme; htCP, high-throughput cell phenotyping; TSA, trichostatin A

[1] Correspondence: The Johns Hopkins University, 3400 N. Charles St., NEB 116, Baltimore, MD 21218, USA. E-mail: wirtz@jhu.edu

doi: 10.1096/fj.12-227108

This article includes supplemental data. Please visit *http://www.fasebj.org* to obtain this information.

genomic methods, requires cells to be detached from their substrate before analysis, therefore, eliminating the ability to simultaneously obtain information about cell phenotypes, including cell and nucleus morphology, cytoskeleton content, *etc.* Moreover, flow cytometry is unsuitable to assess adherent cells. Immunofluorescence and immunohistochemistry resolve these limitations but are low-throughput. As more novel cancer therapies are developed to target the epigenome, it is important to recognize that drug treatment often causes highly diverse cellular responses within different areas of a heterogeneous tumor (16, 17). Techniques to analyze chromatin modifications, thus, may require true high-throughput, single-cell resolution to accurately screen for new therapies.

Here, we developed, tested, and validated a new microscopy-based assay to measure global H3 acetylation levels of thousands of individual cells and simultaneously measure, in the same cells, a wide range of cell phenotypic properties, including cell and nucleus morphology, cytoskeletal content, and cell-cycle phase. Thanks to our ability of measuring simultaneously the DNA content in the nucleus of cells, we also determined the extent of variations in chromatin variations displayed by cells of identical DNA content and quantitatively assessed whether these variations predicted phenotypic variations of the cells. Finally, we determined whether and how global histone acetylation varied with total DNA content in the nucleus, and then quantified the extent of phenotypic variations and associated epigenetic variations within the same cell-cycle phase without error-prone forced cell synchronization.

MATERIALS AND METHODS

Cell culture and drug treatments

C2C12 mouse myoblast cells and MDA-MB-231 breast adenocarcinoma cells were cultured in DMEM (Mediatech, Manassas, VA, USA) supplemented with 10% FBS (HyClone, Logan, UT, USA) and 100 U of penicillin/100 μg of streptomycin (Sigma, St. Louis, MO, USA). All cells were maintained at 37°C in a humidified, 5% CO_2 environment. Cells were passaged every 2–3 d for a maximum of 20 passages.

Trichostatin A (TSA; Sigma) was dissolved in stock dimethyl sulfoxide (DMSO) and then added to the complete culture medium for a final drug concentration of 100 nM. A DMSO control condition was used with an equal volume of DMSO to that used in the drug medium (~1:500).

Cells were seeded overnight in 24-well glass-bottom plates (MatTek, Ashland, MA, USA) at a density of 5000 cells/well. After 16 h, medium was aspirated, and cells were rinsed once with Hank's balanced salt solution (Life Technologies, Carlsbad, CA, USA) before introduction of either control, serum-free, or drug medium. Cells were then allowed to incubate for an additional 24 h before fixation.

Immunofluorescence staining and microscopy

Cells were fixed in 3.7% formaldehyde for 10 min and subsequently permeabilized for 10 min with a PBS solution containing 0.1% sodium azide, 0.5% Triton X-100, and 1% BSA. Cells were then blocked with 10% goat serum in PBS for 1 h before overnight incubation with a primary antibody at 4°C. Anti-acetyl-histone H3 (lys9) and anti-acetyl-histone H4 (lys12) antibodies (EMD Millipore, Billerica, MA, USA) and anti-histone H3 (Sigma) were used at 5 μg/ml. After washing, the cells were incubated for 2 h in a secondary solution containing Hoechst 33342 at 1:50, Alexa Fluor 488 phalloidin at 1:40, and Alexa Fluor 568 goat-anti-rabbit secondary antibody (all from Life Technologies) at 1:200. Fluorescent images were collected using a Luca-R EMCCD camera (Andor Technology, Belfast, UK) mounted on a Nikon TE2000 microscope (Nikon, Tokyo, Japan) with a ×20 Plan Apo objective (N.A. 0.75). Cells were imaged at constant exposure time and the same camera settings within each fluorescent channel. Within each well of the 24-well, glass-bottom plates, a 9 × 9 grid of microscope stage positions with 0.65-mm offset spacing in all directions was scanned for a total of 81 images per well.

Microscope image calibration and analysis

To accurately measure intensity magnitude in the wide-field fluorescent microscopy system, acquired fluorescent images were calibrated *via* two measurements of intensity: background intensity and nonuniform intensity response (18). The background intensity, I_B, was estimated by acquiring an image under no light (no fluorescent excitation) for each fluorescent channel using the same exposure time used for imaging the cells. The nonuniform intensity response is wavelength-dependent and was realized for each fluorescent channel by imaging the intensity distribution, I_{NR}, over different pixels in an aqueous well-mixed solution of Hoechst 33342 and DNA from salmon testes (as Hoechst 33342 only emits fluorescence effectively when bound to DNA), FITC, and Alexa Fluor 568 dye. Following the subtraction of the background intensity, this intensity distribution was further normalized by its mean to obtain the normalized pixel-dependent intensity responsive gain, I_G, from the following equation:

$$I_G = (I_{NR} - I_B)/\langle (I_{NR} - I_B) \rangle$$

Here, $\langle X \rangle$ represents the mean of variable X. The calibrated stained cell images, I_C, were obtained through the following equation from the raw image, I_R:

$$I_C = (I_R - I_B)/I_G$$

A customized MATLAB program segmented cells using phalloidin actin staining, segmented nuclei using Hoechst 33342 DNA staining, and quantified fluorescence intensities in a pixel-by-pixel manner for each fluorescent channel. For both Hoechst 33342 and histone-stained images, intensity parameters were measured only inside the traced nuclear regions. In this manner, DNA content, and therefore cell-cycle phase, was quantified for each nucleus (18, 19). For phalloidin-stained images, intensity was measured only inside the traced cellular regions. Cell and nucleus circularity values were calculated as $4\pi A/P^2$, where A is the area and P is the perimeter of the cellular or nuclear segment. In this manner, circularity ranges from 0 to 1 and approaches 1 for a perfectly circular segment.

To divide cellular populations into cell-cycle phases, DNA summation intensity distributions were normalized by the fluorescence intensity corresponding to the location of the first large peak, assumed to be the G_1 peak. After normalization, any cells with a value of DNA content <1.2 were assumed to be in the G_0/G_1 phase, any cells with a value of DNA content >1.8 were assumed to be in the G_2/M phase,

and any cells with DNA content falling between 1.2 and 1.8 were assumed to be in the S phase. In addition, in order to prevent any cellular debris from being included in analysis, data were gated, such that any recognized objects with normalized DNA content <0.2 or >2.8 were eliminated.

Histone extraction and Western blot analysis

For Western blots, cells were harvested and washed with PBS supplemented with 5 mM sodium butyrate to retain levels of histone acetylation. Cells were lysed with PBS containing 0.5% Triton X-100, 2 mM phenylmethylsulfonyl fluoride, and 0.02% sodium azide. After centrifugation, the pellet was resuspended in 0.2 N hydrochloric acid overnight at 4°C to obtain histones by acid extraction. The Bradford assay was used to determine the protein concentration of each sample so that equal amounts were loaded into the precast 12% polyacrylamide gels (Bio-Rad, Hercules, CA, USA). SDS-PAGE was performed at 250 V for 30 min at 4°C to separate protein samples before transferring gels onto 0.2-μm nitrocellulose membranes (Bio-Rad). Membranes were then blocked with 5% powdered milk in TBS-Tween for 1 h, followed by an overnight primary incubation with 0.05 μg/ml anti-acetyl-histone H3 (EMD Millipore) at 4°C. After 2 h of incubation with secondary antibodies, blots were developed with an Immun-Star HRP chemiluminescence kit (Bio-Rad). Gels were also stained with Coomassie blue as loading controls. Both gels and membranes were imaged with a Bio-Rad ChemiDoc XRS+ imaging system, and all bands were quantified by relative intensity using Bio-Rad Image Lab software. The entire histone extraction and Western blot process was performed on 2 separate occasions from 2 sets of independent biological samples, and relative intensity values were averaged.

Statistical analysis

Mean values, standard error of measurement, and statistical analysis for all data shown were calculated using Microsoft Excel (Microsoft, Redmond, WA, USA) and plotted using GraphPad Prism (GraphPad Software, La Jolla, CA, USA). For all experiments, ≥ 2 independent biological trials were conducted for ≥ 200 cells/condition (see number of cells analyzed for each experiment in the figure captions). Where appropriate, *t* tests or 1-way and 2-way ANOVA analyses with Tukey and Bonferroni posttests were used to compare means; $\alpha = 0.05$ was used for all significance tests.

RESULTS

Simultaneous measurements of cell phenotypes, cell cycle, and chromatin modifications at a single-cell resolution

Even isogenic cells in culture dishes, which provide cells with a biochemically and biophysically uniform environment, tend to display an extremely wide range of cell and nucleus shapes and sizes, chromosomal organizations, cell-cycle duration, and cytoskeletal contents and architectures (20). The underlying molecular mechanisms leading to such wide phenotypic variations are unclear because of the unmet need to combine simultaneous molecular and phenotypic measurements at single-cell resolution. Cell-to-cell phenotypic variations *in vivo* and *in vitro* may stem from genetic and epigenetic variations, as well as variations in molecular compositions of cells in each cell-cycle phase, which are difficult to decouple from one another. Whether isogenic cells of identical DNA content in the same cell-cycle phase present the same global epigenome is unknown. We hypothesized that observed variations in cell phenotypes, in particular, nucleus/cell size and shape and actin filament content in cells in culture, could be explained in part by cellular variations in chromatin modifications.

To analyze acetylation on histone H3 and cell-cycle-dependent cell phenotypes of single, adherent cells, we developed a high-throughput cell phenotyping (htCP) assay capable of measuring global chromatin modifications, DNA content, and a wide range of morphological cell and nuclear properties (**Fig. 1**). C2C12 mouse myoblasts were seeded at controlled low density and allowed to incubate for 1.5 d before being fixed and stained for nuclear DNA using Hoechst 33342, for acetylated histone H3 (AcH3; lys9) or acetylated histone H4 (AcH4; lys12), and for overall histone H3 content using corresponding primary antibodies, and for filamentous actin (F-actin) using phalloidin (Fig. 1*A*, *B*). Cells were scanned using a ×20 microscope objective with 4 fluorescent channels of an automated light microscope. The quantitative calibration and custom software developed to quantify fluorescence intensities to compute DNA content (and therefore cell cycle phase) and global acetylation per cell are detailed in Materials and Methods; >1000 cells were analyzed in <15 min at single-cell resolution.

Delineation of boundaries of cells and nuclei to compute their shape and size were obtained from custom computer-aided segmentation based on the phalloidin stain at the cell periphery and the Hoechst 33342 stain of nuclear DNA. Segmentation was validated by comparing these results to those obtained by manual tracing of the same nuclei and cells (see Materials and Methods and Supplemental Fig. S1*C*, *D*). Application of this single-cell assay allowed for simultaneous measurements of distributions of a variety of parameters relating to histone acetylation (Fig. 1*E–G*), cell cycle (Fig. 1*H*, *I*), and cell and nucleus morphology (Fig. 1*J–N*). Our single-cell assay measured the DNA content of individual C2C12 cells, which at the population level showed the classical distribution in DNA contents delineating the G_0/G_1, S, and G_2/M cycle phases (Fig. 1*H*, *I*). Measurements of fractions of cells in each cell-cycle phase were validated with conventional flow cytometry, which showed quantitative agreement (see Supplemental Fig. S1*E*, *F*).

Cell phenotypes showed wide distributions in all measured parameters, including a ~10-fold range in nuclear size (Fig. 1*J*). The assay also revealed that C2C12 cells showed a ~20-fold range in global H3 acetylation (Fig. 1*F*; validation of measurements of relative histone acetylation is presented below and in Supplemental Fig. S1*A*, *B*) and a ~30-fold range in overall H3 content per cell (Fig. 1*E*). We also generated a normalized histone H3 acetylation parameter by

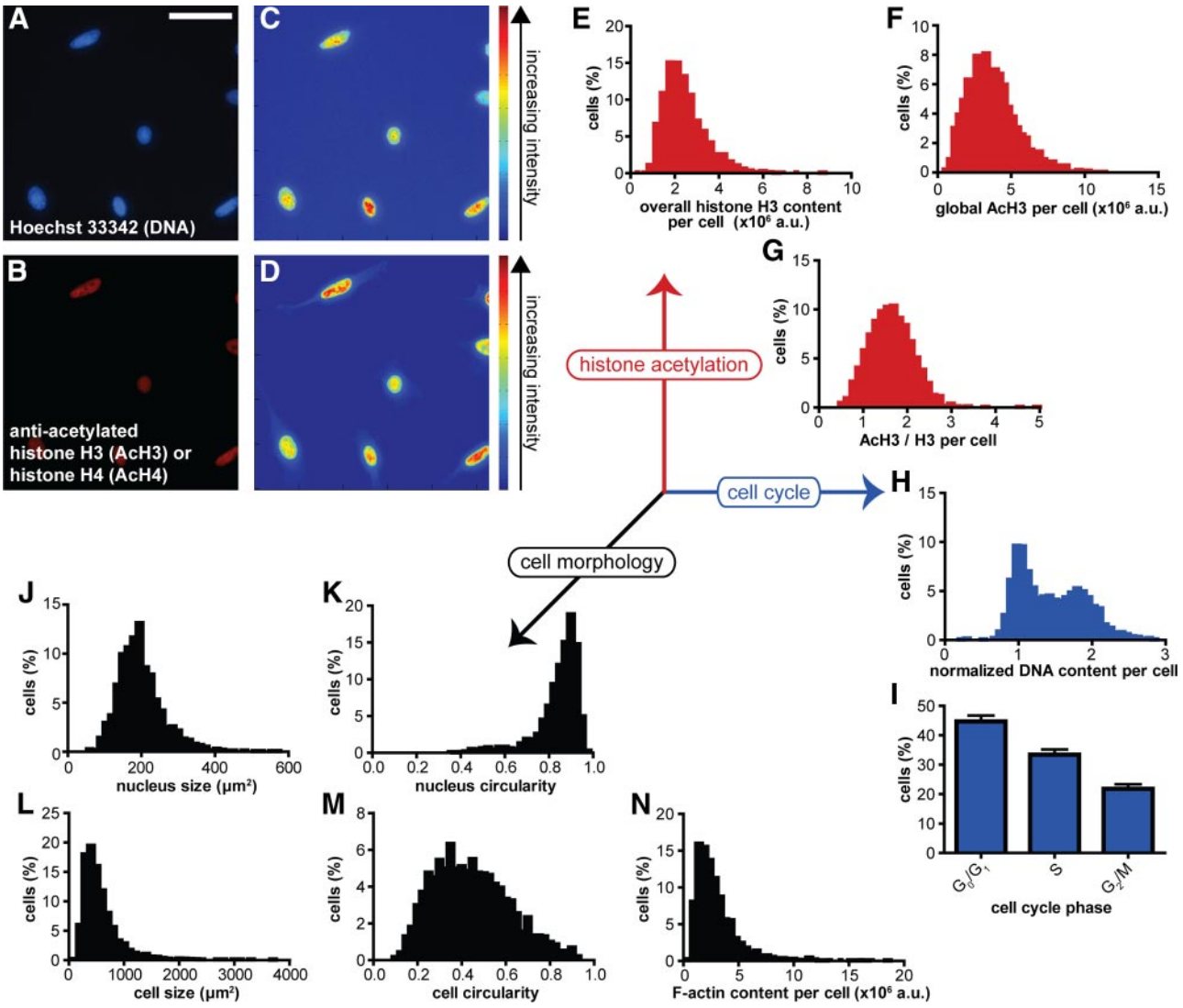

Figure 1. Simultaneous measurements of relative histone acetylation, DNA content, and cell/nucleus morphology at single-cell resolution. *A–D*) Typical micrographs showing nuclear DNA (*A*) and acetylated histone (*B*) stains and corresponding heat maps of DNA intensity (*C*) and histone acetylation intensity (*D*) in each cell. Scale bar = 100 μm. *E–G*) Distributions of overall histone H3 content per cell (*E*), global histone H3 acetylation per cell (*F*), and H3 acetylation normalized by overall histone H3 content per cell (*G*). *H, I*) Distribution of DNA content per cell normalized by the fluorescence intensity at the G_0/G_1 peak (*H*) and the corresponding fraction of cells in the G_0/G_1, S, and G_2/M cell cycle phases (*I*). Panel *I* shows the mean ± SE. *J–N*) Distributions of nucleus size (*J*), nucleus circularity (*K*), cell size (*L*), cell circularity (*M*), and F-actin content per cell (*N*). Two biological repeats of 2 duplicate samples were conducted for a total of 2309 cells for all panels.

taking the ratio of acetylated histone H3 to overall histone H3 content per cell (Fig. 1*G*).

Variations in histone acetylation predict variations in cell and nucleus morphology

We asked whether variations in histone acetylation were predictive of the variations in morphological descriptors of the same cells (**Fig. 2**). We found a positive correlation between global acetylation on histone H3 and DNA content (Fig. 2*A*) and between global H3 acetylation and nucleus size (Fig. 2*B*). These correlations were further verified when the distributions of both DNA content and nucleus size were subdivided into bins, and average global histone H3 acetylation within each bin was statistically compared (inset graphs in Fig. 2). We also observed a less significant positive correlation between global H3 acetylation and cell size (Fig. 2*C*). These correlations may not be surprising, because as cells go through their cell cycle (and DNA content increases), one expects that protein content increases (including histone-associated enzymes) and nuclear size increases. Histone H3 acetylation was found to have no significant correlation with cell circularity (Fig. 2*D*). This last result indicates that not all phenotypic variations can be predicted by variations in histone acetylation.

Variations in normalized degree of acetylated histone

We next asked whether these positive correlations, specifically among global histone H3 acetylation and

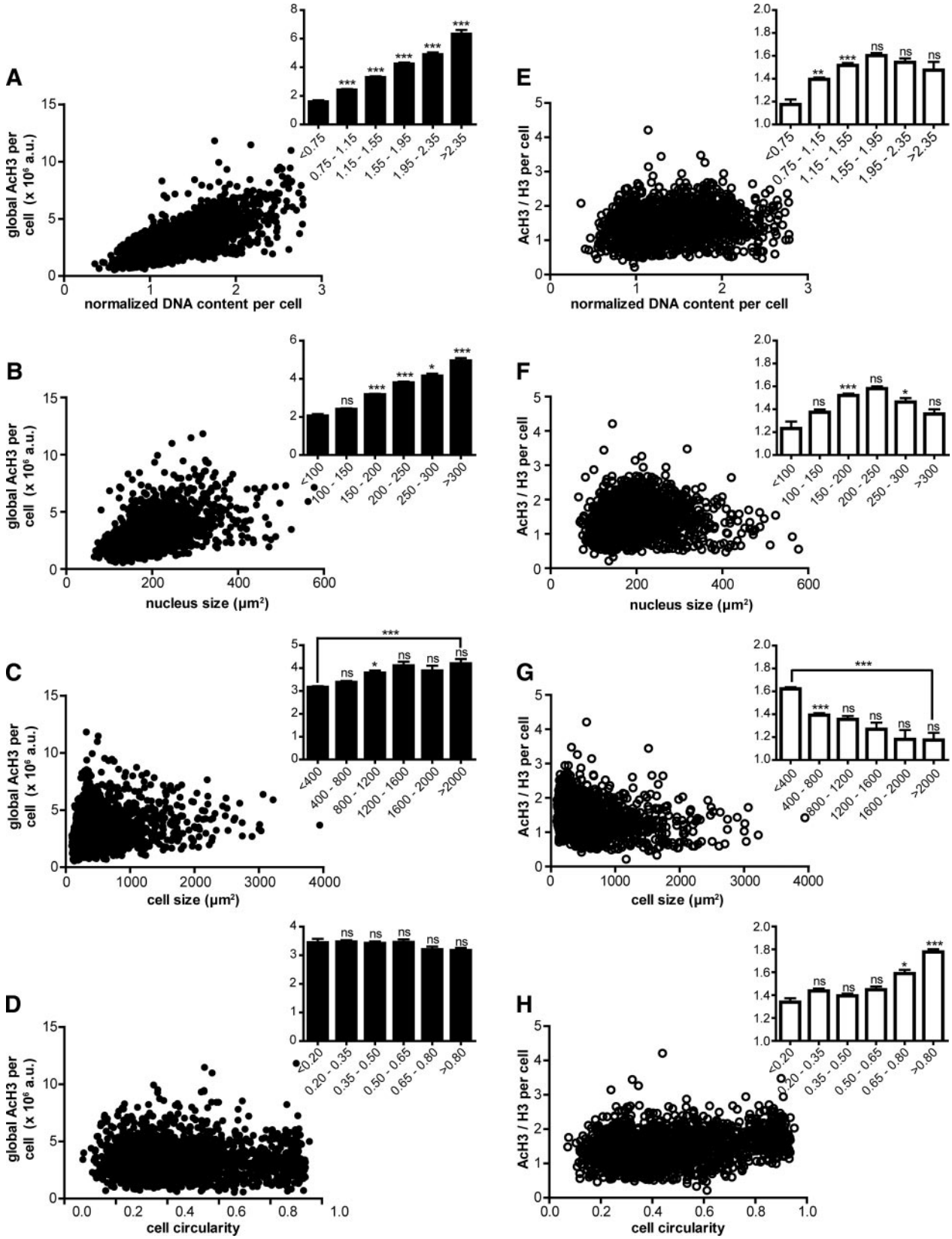

Figure 2. Variations in histone acetylation predict variations in cell and nucleus morphology. *A–D*) Global acetylation on histone H3 as a function of normalized DNA content per cell (*A*), nucleus size (*B*), cell size (*C*), and cell circularity (*D*) at single-cell resolution. *E–H*) Acetylation on histone H3 normalized by overall histone H3 content per cell as a function of normalized DNA content per cell (*E*), nucleus size (*F*), cell size (*G*), and cell circularity (*H*) at single-cell resolution. Insets show the same data binned by the *x*-axis parameter (mean±SE AcH3) and statistically compare each bin to the preceding bin using 1-way ANOVA tests. Two biological repeats of 2 duplicate samples were conducted for a total of 1832 cells for all panels. ns, not significant ($P>0.05$). *$P < 0.05$; **$P < 0.01$; ***$P < 0.001$.

DNA content and nucleus size, were, in fact, due to the overall content of histones increasing proportionally with DNA content and nucleus size, thus making more histones available for acetylation. We, therefore, normalized all global H3 acetylation values by overall H3 content of the same cells, having stained cells with both anti-acetyl histone H3 and anti-histone H3 antibodies simultaneously (Fig. 2*E–H*). After normalization, we found less significance in the relationships that had shown strong correlations before normalization (histone H3 acetylation with DNA, Fig. 2*E*, and histone H3 acetylation with nucleus size, Fig. 2*F*). In fact, these correlations showed maximum acetylation at midpoint values of DNA content and nucleus size, before acetylation began to decrease with larger DNA contents or nucleus sizes. Unexpectedly, normalized histone H3 acetylation decreased with increasing cell size (Fig. 2*G*). Moreover, normalized histone H3 acetylation showed a strong correlation with cell circularity when cell circularity was >0.5 (Fig. 2*H*). We note that cell circularity (shape) is a feature of adherent cells that becomes meaningless if assessed by conventional methods, such as flow cytometry, since cells become essentially spherical when they are artificially detached from their substrate.

Variations in chromatin modifications for cells of same DNA content and same nucleus size

Although global histone acetylation was positively correlated with DNA content (Fig. 2*A*) and nuclear size (Fig. 2*B*), we asked whether these parameters would still vary for cells of highly similar DNA content or nuclear size, without additional cell manipulation. From the DNA content distribution (Fig. 1*H*), we isolated a narrow sleeve of cells within each of the three cell cycle phases G_0/G_1, S, and G_2/M (**Fig. 3*A***), with each sleeve encompassing only 2–3% of the total range in DNA contents displayed by the entire cell population. Then, having held DNA content essentially constant, we examined the corresponding distributions of nucleus size (Fig. 3*B*), global acetylation of histone H3 (AcH3, Fig. 3*C*), and AcH3 normalized by overall histone H3 (Fig. 3*D*) within each sleeve and compared these distributions to the whole cell population (gray bars, Fig. 3). Remarkably, a narrow span in DNA contents corresponded to wide spans of up to 77% of all measured nuclear size values (~4-fold variations), 88% of all global AcH3 values (~7-fold variations), and 86% of all normalized AcH3 values (~6-fold variations, see Supplemental Table S1).

Similarly, narrow sleeves of nucleus size (Fig. 3*E–H*), global AcH3 (Fig. 3*I–L*), and AcH3 normalized by overall H3 (Fig. 3*M–P*) were isolated, and the remaining 3 distributions were compared. Again, relatively large variations were observed in the 3 remaining parameters when 1 parameter was held essentially constant (Supplemental Table S1).

We asked whether the positive correlations observed in Fig. 2 held true within these narrow population slices. Although global AcH3 did not correlate with nucleus size in the narrow G_0/G_1, S, and G_2/M DNA slices (Fig. 3*Q*), DNA content correlated with nucleus size when AcH3 was held constant (Fig. 3*R*), and AcH3 correlated with DNA content when nucleus size was held constant (Fig. 3*S*). These findings show the remarkable result that cells not only within the same phase of the cell cycle, but with essentially identical DNA content cultured in identical conditions, can still display a wide range of variations in chromatin-associated modifications, and these variations predict DNA content and nucleus size variations. We also note that the htCP assay measures cell phenotypes and histone acetylation in each phase of the cell cycle without forced cell synchronization using drugs, which are prone to artifacts by unintentionally affecting many other signaling pathways within the cell.

Cell cycle-dependent histone acetylation following pharmacological treatment

To further demonstrate the versatility of our assay, we next asked what a cell treatment or stimulation intending to change one set of parameters would have on the other parameters. For instance, to affect DNA content and, therefore, cell cycle distribution, C2C12 cells were serum starved for 24 h, which is known to enrich cells in the G_0/G_1 phase, as confirmed (**Fig. 4*A***, red curve; *B*, red bars). Serum starvation also significantly increased nuclear size (Fig. 4*C*, red bars) but, surprisingly, had little effect on global histone H3 acetylation (Fig. 4*D*, red bars). After normalization with overall histone H3 content, however, acetylation was significantly lessened by serum starvation (Fig. 4*E*, red bars). Serum starvation also significantly decreased F-actin content (Fig. 4*F*).

To purposefully alter histone acetylation, C2C12s were separately treated with TSA, a known HDAC inhibitor, for 24 h. TSA treatment greatly increased both unnormalized and normalized histone H3 acetylation (Fig. 4*D*, *E*, purple bars) relative to treatment with the drug vehicle DMSO as a control (Fig. 4*D*, *E*, green bars). TSA treatment also dramatically shifted cell-cycle distribution to the G_0/G_1 phase (Fig. 4*A*, purple curve; *B*, purple bars), increased nucleus size by almost 50% (Fig. 4*C*, purple bars), and almost doubled F-actin content (Fig. 4*F*, purple bars). These results illustrate the ability of our method to successfully measure histone acetylation, cell cycle distribution, and cell/nuclear morphology simultaneously in the same cells across a wide variety of conditions.

To further illustrate the applicability of the htCP assay, we subjected a different cell line, MDA-MB-231 human breast adenocarcinoma cells, to the analysis described above. Our assay revealed a wide distribution of global acetylation on histone H3 complemented by positive correlations with DNA content and nucleus size (Supplemental Fig. S2).

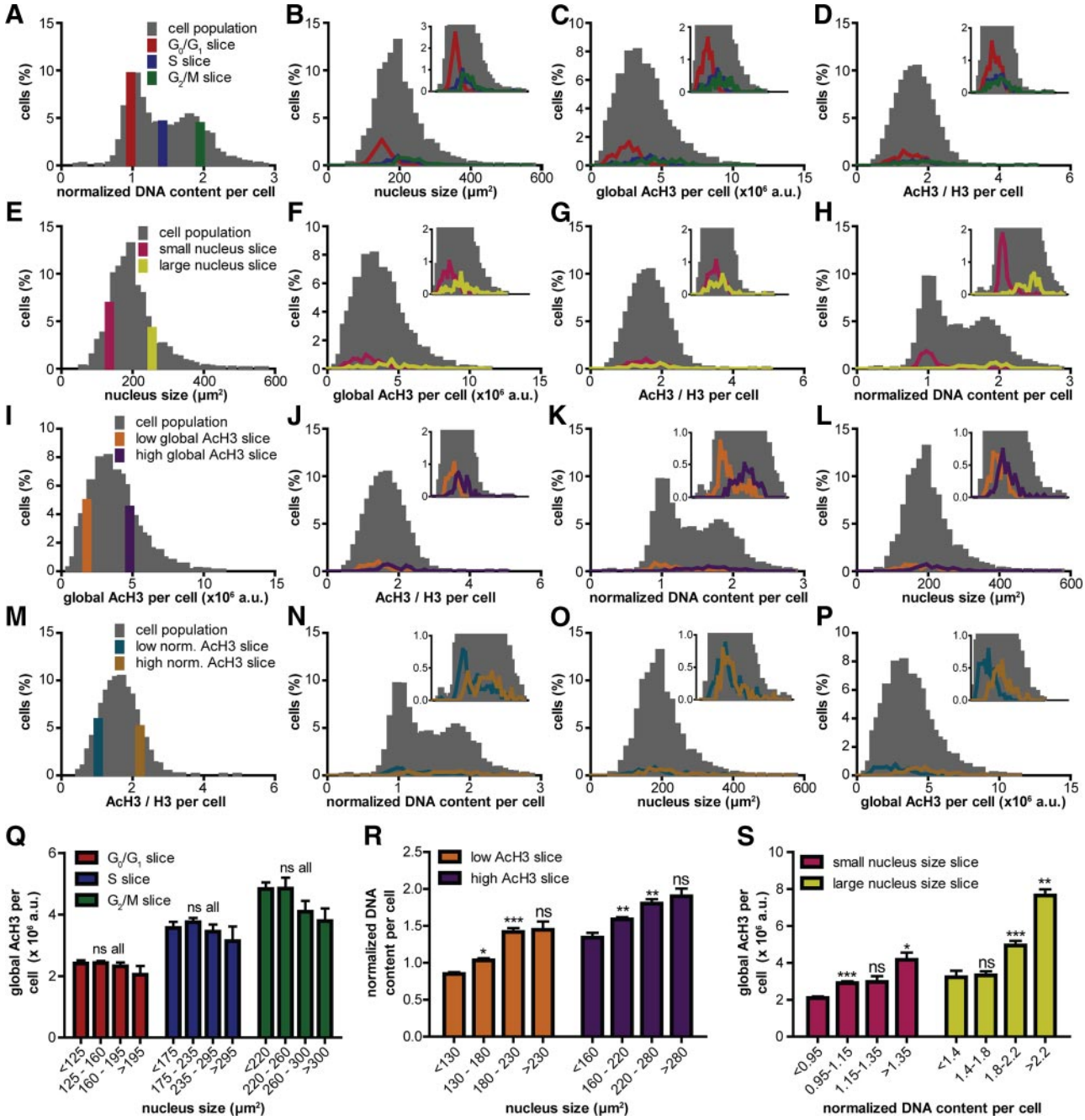

Figure 3. Heterogeneities in histone acetylation and nucleus size as a function of DNA content. *A*) Narrow slices were computationally isolated from the DNA content distribution at each of the 3 cell cycle phases, G_0/G_1 (red, 221 cells), S (blue, 105 cells), and G_2/M (green, 101 cells). *B–D*) Distributions of nucleus sizes (*B*), histone H3 acetylation values (*C*), and histone H3 acetylation normalized by overall histone H3 content (*D*) were plotted for the whole cell population (gray bars) and for the cells in each of the 3 DNA content slices. *E*) Narrow slices were isolated from the nucleus size distribution at small nucleus size (pink, 158 cells) and large nucleus size (yellow, 97 cells). *F–H*) Distributions of global AcH3 values (*F*), normalized AcH3 values (*G*), and DNA contents (*H*) were plotted for the whole cell population (gray bars) and for the cells in each of the 2 nucleus size slices. *I*) Narrow slices were isolated from the global AcH3 distribution at low acetylation (orange, 114 cells) and high acetylation (purple, 103 cells). *J–L*) Distributions of normalized AcH3 values (*J*), DNA contents (*K*), and nucleus sizes (*L*) were plotted for the whole cell population (gray bars) and for the cells in each of the two AcH3 slices. *M*) Narrow slices were isolated from the normalized AcH3 distribution at low (teal, 135 cells) and high values of normalized acetylation (brown, 118 cells). *N–P*) Distributions of DNA contents (*N*), nucleus sizes (*O*), and AcH3 values (*P*) were plotted for the whole cell population (gray bars) and for the cells in each of the 2 normalized AcH3 slices. For panels *A–P*, insets show the same data with the *y* axis magnified to better show distributions. *Q*) Global histone H3 acetylation plotted with binned values of increasing nucleus size for each narrow slice of DNA content. *R*) DNA content plotted with binned values of increasing nucleus size for each narrow slice of global histone H3 acetylation. *S*) Global histone H3 acetylation plotted with binned values of increasing DNA content for each narrow slice of nucleus size. For panels *Q–S*, bars show means ± SE, and statistics compare bars to the preceding bar using 1-way ANOVA tests. For all panels, two biological repeats of two duplicate samples were conducted for a total of 2309 cells in the overall population. ns, not significant ($P>0.05$). *$P < 0.05$; **$P < 0.01$; ***$P < 0.001$.

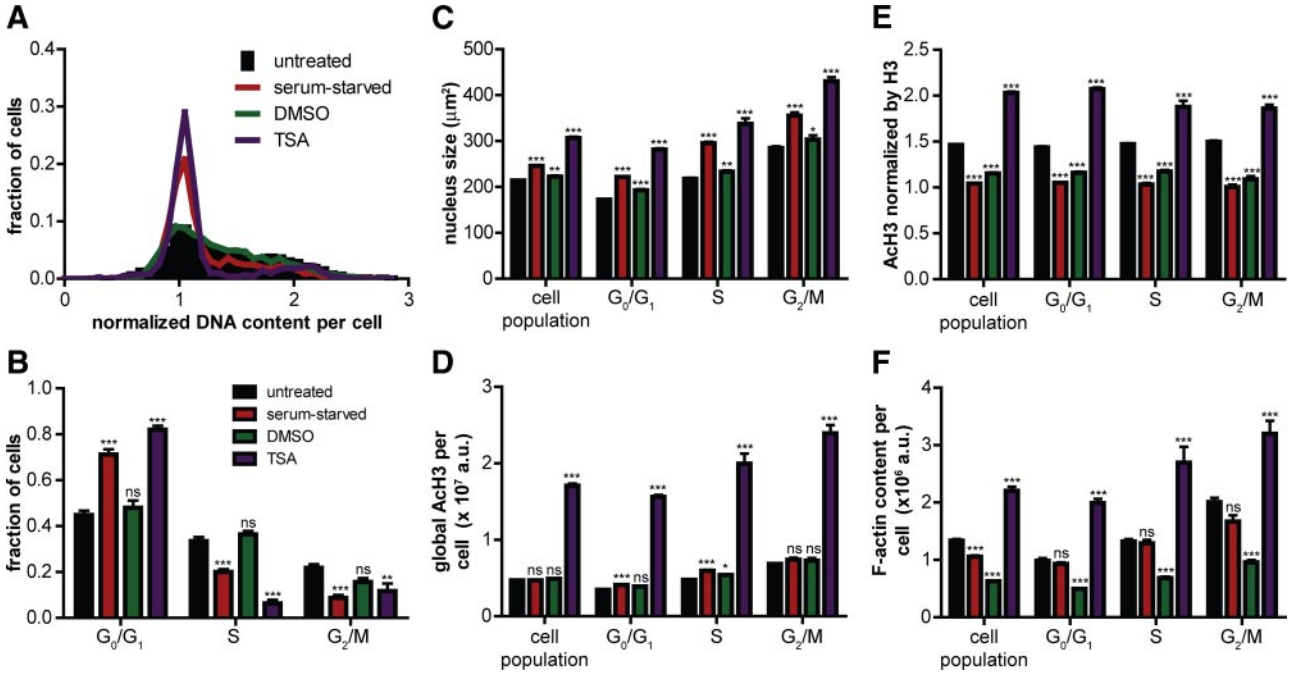

Figure 4. Histone acetylation as a function of cell cycle. *A*) Cell-cycle distribution of untreated control cells (black bars), compared to that of serum-starved cells (red curve), TSA-treated cells (purple curve), and DMSO-treated cells (the drug-vehicle control for TSA, green curve). *B*) Corresponding fractions of cells in the G_0/G_1, S, and G_2/M cell cycle phases for each of the 4 conditions. *C–F*) Average nucleus size (*C*), global histone H3 acetylation (*D*), histone H3 acetylation normalized by overall histone H3 content (*E*), and F-actin content (*F*) for the whole cell population, as well as within each of the cell cycle phases for the same 4 conditions. For panels *B–F*, bars show means ± SE, and statistics compare each condition to the untreated control (black bars) using 2-way ANOVA tests. For all panels, 2 biological repeats of 2 duplicate samples were conducted for a total of 2337 untreated cells, 1341 serum-starved cells, 849 DMSO-treated cells, and 801 TSA-treated cells. ns, not significant ($P>0.05$). $*P < 0.05$; $**P < 0.01$; $***P < 0.001$.

Validation with conventional Western blot-based measurements

To validate our assay and verify that the overall changes in histone acetylation measured by this single-cell method were correct at the cell-population level, histones were extracted, and acetylated histone H3 expression was quantified by conventional Western blot in untreated, serum-starved, DMSO-treated (TSA vehicle control), and TSA-treated cells, using Coomassie blue as a loading control. Relative to AcH3 expression in untreated cells, the htCP method presented here and Western blotting produced generally similar results (Supplemental Fig. S1*A*, *B*). Slight differences may be accounted for by cell density, as our htCP assay used a controlled low-seeding density, while a much higher seeding density was needed to obtain enough cells to perform Western blots. In addition, Coomassie blue analysis indicated a slightly lower loading of serum-starved histone extracts for the Western blots, even after the Bradford assay was used to determine equivalent loading amounts.

Variations in histone H3 acetylation predict variations in F-actin content

We next related histone acetylation and DNA content to other important properties of cells besides morphology and cell cycle phase, including the cytoplasmic content in F-actin within each cell. Again, actin filament content and organization cannot accurately be assessed by flow cytometry, as detaching adherent cells from their substrate changes cell shape and significantly affects these cytoskeletal parameters. Bins of increasing global AcH3 per cell and DNA content per cell both revealed increased cytoplasmic content in F-actin per cell (Supplemental Fig. S3*A*, *B*). Cells with relatively low histone H3 acetylation tended to have low DNA content and low F-actin content (Supplemental Fig. S3*C*, *E*, *G*), while cells with relatively high histone H3 acetylation tended to have high DNA content and high F-actin content (Supplemental Fig. S3*D*, *F*, *H*). This result suggests that changes in F-actin content are significantly predicted by variations in histone H3 acetylation.

Interestingly, after global AcH3 was normalized by overall histone H3 content (Supplemental Fig. S3*I*), a negative relationship was observed, suggesting that cells with the highest ratio of histone H3 acetylation to overall histone H3 had the lowest F-actin content. In addition, F-actin was found to strongly relate with cell and nuclear morphology (Supplemental Fig. S3*J–L*), as cells with the largest nuclei and the largest, most elongated cell bodies had the highest F-actin content.

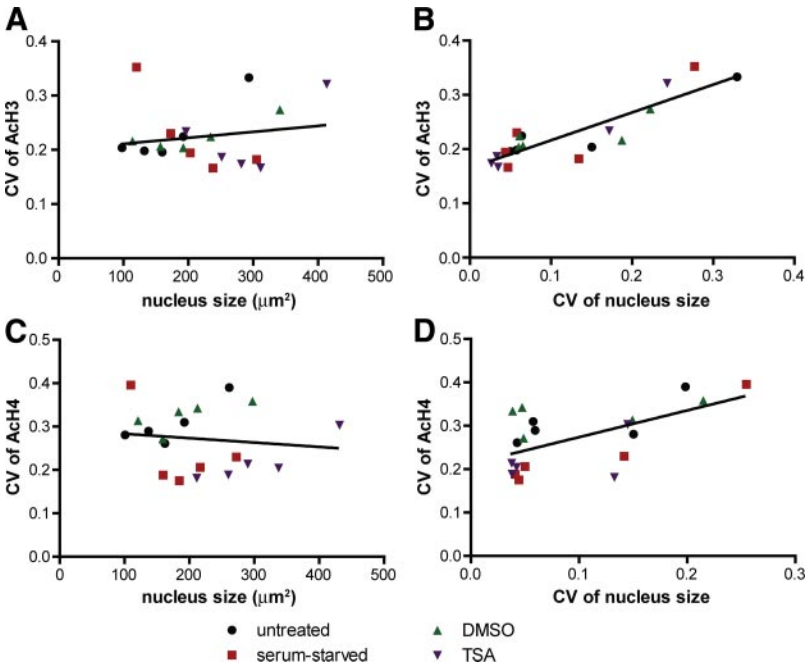

Figure 5. Cellular variations in histone acetylation predict phenotypic variations. *A*, *B*) Coefficient of variation (CV) of acetylated histone H3 values as a function of nucleus size (*A*) and as a function of CV of nucleus size (*B*) for 5 subpopulations of each of the 4 listed conditions. CV of acetylated histone H4 values as a function of nucleus size (*C*) and as a function of CV of nucleus size (*D*) for 5 subpopulations of each of the 4 listed conditions. Black lines show the best-fit line through all 20 points for each plot. For panels *A* and *B*, 2 biological repeats of 2 duplicate samples were conducted for a total of 1301 untreated cells, 810 serum-starved cells, 838 DMSO-treated cells, and 417 TSA-treated cells. Each population was divided into 5 subpopulations by binned nucleus size. For panels *C* and *D*, 2 biological repeats of 2 duplicate samples were conducted for a total of 1100 untreated cells, 676 serum-starved cells, 1212 DMSO-treated cells, and 214 TSA-treated cells.

Variations in histone acetylation predict phenotypic variations

Finally, we asked whether variations in histone acetylation among a population of cells could be predictive of variations in phenotypic parameters, addressing the main hypothesis of this study. Data sets for the 4 conditions tested in this study (untreated, serum starved, DMSO treated, and TSA treated) were divided into 5 equal subpopulations based on binned nucleus sizes. For each of these 20 subpopulations, the coefficient of variation (CV) of the AcH3 intensity distribution within the subpopulation was plotted as a function of both the average nucleus size in the subpopulation (**Fig. 5*A***) and the CV of nucleus sizes within the subpopulation (Fig. 5*B*). Cell-to-cell variations in global acetylation were observed to be independent of nucleus size, but significantly increased with variations in nucleus size in that cell population. Moreover, to test whether these results held true for other histones, we replaced the anti-acetyl H3 antibody with an anti-acetyl histone H4 antibody and performed the same analysis. Results for histone H4 acetylation variations were very similar to those of histone H3 acetylation variations (Fig. 5*C*, *D*).

DISCUSSION

We have introduced and fully validated a combined assay that measures global H3/H4 histone acetylation at single-cell resolution, while simultaneously measuring important cell properties, including F-actin cytoplasmic content, cell-cycle phase (DNA content per nucleus), and cell and nuclear shape and size of thousands of cells. This assay does not require detachment of cells from their substrate, preserves the microenvironment of the cells (*e.g.*, cell density), and, therefore, preserves normal cell and nuclear properties of adherent cells, which allowed us to test long-standing questions in biology. Application of this assay on mouse myoblasts and human breast cancer cells reveals that, despite an identical biochemical and biophysical milieu, cells display extremely wide ranges of phenotypes, as well as levels of histone content and acetylation. This assay shows that variations in acetylation on histones H3 and H4 predict variations in nuclear size. We note that established cell lines, especially those of cancer origin, tend to develop aneuploidy (21), and this may account for some of the cellular heterogeneity observed in our studies. Future work will analyze epigenetic heterogeneity in primary cell lines that are believed to have more uniform cellular populations.

We anticipate that this method will benefit the screening of cancer drugs targeting the epigenome. Tumors can consist of heterogeneous cell subpopulations (16, 17), each of which may react to drugs differently, thus creating a large obstacle to overcome for the development of successful treatments. Our single-cell method of studying chromatin modifications complements other single-cell and genomic methods and could be used to monitor the effectiveness of potential cancer therapies, such as HDAC inhibitors. Trichostatin A and another assumedly similar HDAC modulator, depsipeptide, were recently demonstrated to result in very distinct activity with respect to cell viability and histone modifications across several cancer types (22). Large-scale studies combining varieties of potential therapies such as these with heterogeneous populations of cells could be beneficial in developing specific, personalized treatments for individual cancer patients. Extensions of the htCP assay to measure DNA and histone methylation are under way. FJ

The authors thank Prof. Jonathan Licht (Northwestern University, Chicago, IL, USA) for fruitful conversations and Dr. Sean Hanlon (U.S. National Cancer Institute, Bethesda, MD, USA) for important suggestions and editing the manuscript. This work was supported by U.S. National Institutes of Health grants R01CA174388 and U54CA143868. A.B.C. is supported by an Achievement Rewards for College Scientists (ARCS) Foundation fellowship.

REFERENCES

1. Strahl, B. D., and Allis, C. D. (2000) The language of covalent histone modifications. *Nature* **403,** 41–45
2. Zhang, K., and Dent, S. Y. R. (2005) Histone modifying enzymes and cancer: going beyond histones. *J. Cell. Biochem.* **96,** 1137–1148
3. De Ruijter, A. J., van Gennip, A. H., Caron, H. N., Kemp, S., and van Kuilenburg, A. B. (2003) Histone deacetylases (HDACs): characterization of the classical HDAC family. *Biochem. J.* **370,** 737–749
4. Esteller, M. (2008) Molecular origins of cancer: epigenetics in cancer. *N. Engl. J. Med.* **358,** 1148–1159
5. Sharma, S., Kelly, T. K., and Jones, P. A. (2010) Epigenetics in cancer. *Carcinogenesis* **31,** 27–36
6. Portela, A., and Esteller, M. (2010) Epigenetic modifications and human disease. *Nat. Biotechnol.* **28,** 1057–1068
7. Seligson, D. B., Horvath, S., Shi, T., Yu, H., Tze, S., Grunstein, M., and Kurdistani, S. K. (2005) Global histone modification patterns predict risk of prostate cancer recurrence. *Nature* **435,** 1262–1266
8. Witt, O., Deubzer, H. E., Milde, T., and Oehme, I. (2009) HDAC family: What are the cancer relevant targets? *Cancer Lett.* **277,** 8–21
9. Fraga, M. F., Ballestar, E., Villar-Garea, A., Boix-Chornet, M., Espada, J., Schotta, G., Bonaldi, T., Haydon, C., Ropero, S., Petrie, K., Iyer, N. G., Perez-Rosado, A., Calvo, E., Lopez, J. A., Cano, A., Calasanz, M. J., Colomer, D., Piris, M. A., Ahn, N., Imhof, A., Caldas, C., Jenuwein, T., and Esteller, M. (2005) Loss of acetylation at Lys16 and trimethylation at Lys20 of histone H4 is a common hallmark of human cancer. *Nat. Genet.* **37,** 391–400
10. Bolden, J. E., Peart, M. J., and Johnstone, R. W. (2006) Anticancer activities of histone deacetylase inhibitors. *Nat. Rev. Drug Discov.* **5,** 769–784
11. Minucci, S., and Pelicci, P. G. (2006) Histone deacetylase inhibitors and the promise of epigenetic (and more) treatments for cancer. *Nat. Rev. Cancer* **6,** 38–51
12. Chavez-Blanco, A., Segura-Pacheco, B., Perez-Cardenas, E., Taja-Chayeb, L., Cetina, L., Candelaria, M., Cantu, D., Gonzalez-Fierro, A., Garcia-Lopez, P., Zambrano, P., Perez-Plasencia, C., Cabrera, G., Trejo-Becerril, C., Angeles, E., and Duenas-Gonzalez, A. (2005) Histone acetylation and histone deacetylase activity of magnesium valproate in tumor and peripheral blood of patients with cervical cancer. A phase I study. *Mol. Cancer* **4,** 22
13. Ronzoni, S., Faretta, M., Ballarini, M., Pelicci, P., and Minucci, S. (2005) New method to detect histone acetylation levels by flow cytometry. *Cytometry A* **66A,** 52–61
14. Esteller, M. (2007) Cancer epigenomics: DNA methylomes and histone-modification maps. *Nat. Rev. Genet.* **8,** 286–298
15. Dasgupta, A., Sharma, P., and Haque, S. J. (2006) Promoter-specific chromatin immunoprecipitation: A novel method to study the epigenetics of brain tumor cells. *Neuro-Oncol.* **8,** 395–395
16. Heppner, G. H. (1984) Tumor heterogeneity. *Cancer Res.* **44,** 2259–2265
17. Marusyk, A., and Polyak, K. (2010) Tumor heterogeneity: causes and consequences. *Biochim. Biophys. Acta* **1805,** 105–117
18. Chen, W. C., Wu, P. H., Phillip, J. M., Khatau, S. B., Choi, J. M., Dallas, M. R., Konstantopoulos, K., Sun, S. X., Lee, J. S., Hodzic, D., and Wirtz, D. (2013) Functional interplay between the cell cycle and cell phenotypes. *Integr. Biol.* **5,** 523–534
19. Wu, P. H., Hung, S. H., Ren, T., Shih, I. M., and Tseng, Y. (2010) Cell cycle-dependent alternation in NAC1 nuclear body dynamics and morphology. *Phys. Biol.* **8,** 015005
20. Lazarides, E., and Weber, K. (1974) Actin antibody: the specific visualization of actin filaments in non-muscle cells. *Proc. Natl. Acad. Sci. U. S. A.* **71,** 2268–2272
21. Holland, A. J., and Cleveland, D. W. (2012) Losing balance: the origin and impact of aneuploidy in cancer. *EMBO Rep.* **13,** 501–514
22. Chang, J., Varghese, D. S., Gillam, M. C., Peyton, M., Modi, B., Schiltz, R. L., Girard, L., and Martinez, E. D. (2012) Differential response of cancer cells to HDAC inhibitors trichostatin A and depsipeptide. *Brit. J. Cancer* **106,** 116–125

Received for publication January 17, 2013.
Accepted for publication March 18, 2013.